



Impregnation quality diagnosis in Resin Transfer Moulding by machine learning

J. Mendikute^{a,*}, J. Plazaola^b, M. Baskaran^a, E. Zugasti^b, L. Aretxabaleta^a, J. Aurrekoetxea^a

^a Mechanical and Industrial Production Department, Mondragon Unibertsitatea, 20500, Arrasate-Mondragón, Spain

^b Data Analysis and Cybersecurity Group, Mondragon Unibertsitatea, 20500, Arrasate-Mondragón, Spain

ARTICLE INFO

Keywords:

Supervised learning
Quality diagnosis
Composites manufacturing
Resin transfer moulding

ABSTRACT

In recent years, several optimization strategies have been developed which reduce the overall defectiveness of the RTM manufactured part. RTM filling simulations showed that, even using optimized injection strategies, local variations in permeability could still generate local defects in the part. Such defects must be identified quickly and accurately right after the injection phase in order to repair or scrap the part. The present paper analyses the feasibility of diagnosing the quality after the injection stage of RTM parts by Machine Learning. The diagnosis was performed using a Supervised Learning binary classification model trained with synthetic data set. Among the different predictive models studied, Extreme Gradient Boosting and Light Gradient Boosting Machine were the most accurate models for predicting the filling quality of RTM, with an accuracy of 84.9% and 83.35%, respectively. In addition, a scaling of the ML model allowed not only to predict the quality of the part but also to locate the areas where the defect was generated. The computation time of the trained ML model versus the FEM model, both computed with a workstation (CPU Intel Xeon Processor E5.2690 with 2.9 GHz–8 core), were compared. In the specific case studied, a reduction from 360 s to 1 s was observed in the computation time utilizing the trained ML model. Thus, Supervised Learning predictive models can be used for diagnosing the composite quality. They are fast enough to be integrated in real processes and could be helpful for designing the monitoring system.

1. Introduction

The interest in Carbon Fibre Reinforced Plastics (CFRP) is increasing in applications where lightweight design is strategic. CFRP have been extensively used in aeronautics, where properties such as specific stiffness and strength, as well as corrosion resistance, are appreciated [1]. The automotive industry is also seeking massive usage of CFRP, but the high operational costs associated with their manufacturing processes limit a wider application in the sector [2]. Liquid Composite Moulding (LCM) processes, and especially Resin Transfer Moulding (RTM), are competitive for overcoming these challenges [3]. RTM is a processing method with the potential for producing low-cost and geometrically complex automotive composite parts [4]. Nonetheless, RTM process robustness is a challenge, as the part quality is affected by the intrinsic manufacturing uncertainties (fabric reinforcement, matrix material and process parameters variations) [5].

In RTM, a resin is injected into a mould cavity, where a porous dry textile preform has been previously placed. Local variations of

permeability, caused by the multiscale geometric variations of the preform [6], induce impregnation defects such as dry zones and voids. Consequently, to ensure the quality of the final part, complex and time-consuming Non-Destructive Inspection (NDI) operations are required. The cost of these NDI operations can reach 15% of the value of the final component [7]. As impregnation related defects reduce the mechanical properties, severe acceptance criteria (less than a 1% of void content [8]) are imposed, resulting in costly rework or scrappage. Additionally, more conservative part designs which do not enhance the lightweight potential of CFRP are applied [9].

Smart manufacturing approach can enable zero defect manufacturing (ZDM) [10]. For that, the production system must acquire sufficient information from the process and be able to adjust the process in real time. In other words, it must build a digital twin of the physical world and accurately recreate the RTM process [11].

For digital model generation, numerical simulation technology is widely used in RTM, since flow, cure and mechanical models optimize the manufacturing process [4]. For this approach, a thorough knowledge

* Corresponding author.

E-mail address: jmendikute@mondragon.edu (J. Mendikute).

of material properties and the process itself is needed. Furthermore, they are based on generalised boundary conditions that do not take into consideration the fluctuations of the preform permeability of each part.

It is therefore necessary to know the real status of the process through monitoring and data acquisition. Several data acquisition systems are used for RTM, but pressure sensors are particularly advantageous [12]. It is possible to associate pressure values measured at discrete points with resin flow-front position at any time [13]. Additionally, by injecting gas prior to the resin injection, the real local permeability of each preform can be determined by analysing the pressure sensors signals [14]. The pressure evolution in the resin during the filling stage can be related to the void formation [15], but in order to detect hidden patterns data-based modelling are needed.

Data Analysis, such as Machine Learning (ML), has demonstrated to be well aligned with the ZDM philosophy [16]. ML algorithms can operate with high-dimensional multi-variate data and allow extracting implicit patterns from dynamic and large-scale data sets [17]. This enables future predictions and data-driven decisions to be made. There are different ML approaches: Supervised Learning (SL), Unsupervised Learning, Semi-Supervised Learning and Reinforcement Learning. In manufacturing processes, there is a huge amount of data, but their interdependencies are complex and patterns are not obvious. For this reason, SL is the most widely used ML technique in the industry [18]. SL fits a model from previously labelled data in order to make future predictions, which can be a regression or a classification. Whereas regression gives a numerical value, classification predicts categorical class label (binary or multi-label classification) making suitable for quality diagnosis [10].

The accuracy of ML techniques often requires large amounts of data for better generalization and accuracy, which is scarce in the case of RTM. Generating this data experimentally is an expensive and time-consuming approach; additionally the uncertainties that occur during the process can limit the usage of this data. An alternative solution is to generate synthetic data by numerical simulation based on the conventional Finite Element Method (FEM). Data scarcity is solved by synthetic data in different process optimization [19,20] and structural validation scenarios [21,22]. FEM and ML techniques are combine in order to validate prediction and optimization methodologies [19]. To ensure that the ML prediction is reliable, the FEM model on which it is based must be as close to reality as possible, which requires a previous characterization of the process and materials.

When building ML models, the classification algorithm must be selected as well as the value of its hyper-parameters. This is a very time consuming task, as many combinations need to be tried in order to find the most efficient algorithm and hyper-parameters. In response to this,

Automated Machine Learning (Auto-ML) technology is gaining relevance, since it automates the most sensitive phases of the machine learning process [23].

The potential of ML for composite materials has begun to be explored in recent years [24]. ML techniques have been used for composite design and stacking optimization [25,26], NDI techniques for properties assessment [27–29] and for the prediction of mechanical performance [30,31]. Among the composite manufacturing processes, ML has been used for the optimization of The Automated Fibre Placement (AFP) processes [32,33] and for bond strength quality prediction in a hybridisation of thermoforming and over-moulding injection processes [34]. Regarding LCM processes Gonzalez et al. [35] explored the utility of ML, Convolutional Neural Networks (CNN), for predicting the location and size of permeability disturbances based on supervised regression. However, CNN models have shown not to be the most suitable for analysing time series, and they have not provided any criteria for the diagnosis of the RTM parts' quality.

The main contribution of this paper is the development and validation of a predictive model based on supervised learning for the diagnosis of defects in RTM filling stage. Numerical simulation results of the resin injection stage were used as synthetic data for training and validating the model. The selected case study was a rectangular plate segmented in 32 zones with local variations of permeability.

2. Methodology

The main objective was the implementation of a predictive model based on supervised learning to classify the quality of the voids and the unfilled zones of a RTM composite parts. For this purpose, the guidelines of The Cross Industry Standard Process for Data Mining (CRISP-DM) approach [36] were followed. The CRISP-DM methodology determines that between the definition of the problem and its final deployment, four phases must be followed (Fig. 1): Data acquisition, data pre-processing, model training, and model evaluation.

In the data acquisition phase, synthetic data was gathered using the numerical simulation method of the RTM process. The objective of this phase was to generate different scenarios of the RTM process by introducing local permeability variation that generated different quality outputs (voids and unfilled zones). The part to be manufactured was a rectangle segmented in 32 zone, but the four corner zones (vent ports location) were not considered in the quality analysis. Each zone was assigned a permeability from two possible values (with and without binder, K_{bin} and K_{ref} , respectively). The resulting 28 zones and 2 possible permeability values for each zone give 268,435,455 possible combinations. Within all these possible combinations, they were classified into

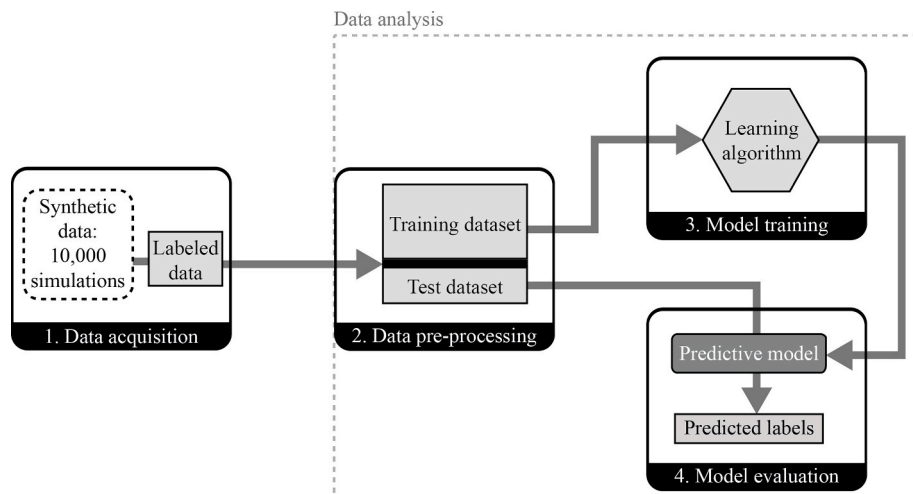


Fig. 1. The scheme of Cross-Industry Standard.

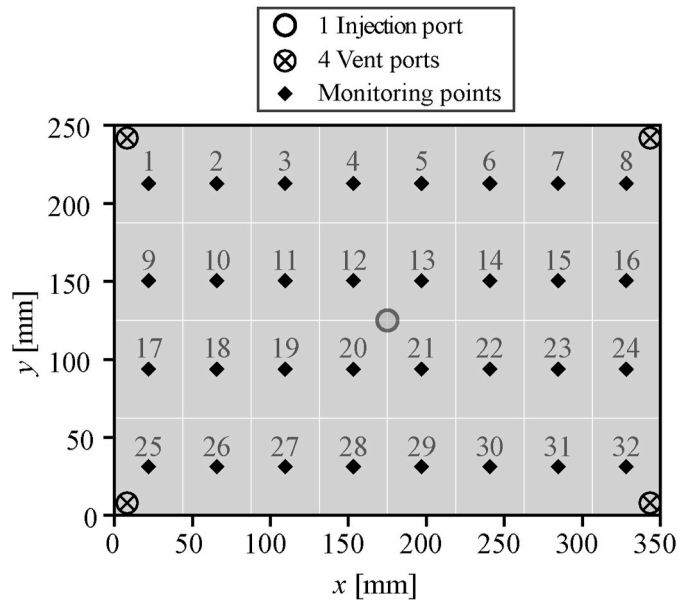


Fig. 2. Scheme of the rectangular plate with.

groups according to the number of zones with K_{bin} permeability (n -group). That is, “3-group” had 3 zones with K_{bin} permeability and the 25 with K_{ref} permeability. To limit the cases, a maximum of 400 simulations were randomly selected from each n -group. Thus, 10,014 simulations were carried out. In each of the simulations, injection flow-rate and the pressure time series at the central point from the 28 zones were recorded. Each simulation was labelled as good/defective quality according to the void content and filling factor criteria. A part was considered defective if it had, at least, one zone with a void content higher than 1% or a filling factor lower than 99.5%.

Then, in the pre-processing phase, flow-rate and pressure time series were processed and structured to obtain their descriptive features by analysing them in the time, frequency and Hilbert domains. Recursive Feature Elimination (RFE) reduction technique was applied to select the most important features without losing performance [37]. Once the data was structured, it was split into training dataset and testing dataset, the 80% and the 20% of the data respectively.

In supervised learning, model training is defined as the phase in which the machine learning algorithm builds a predictive model that relates the input features with target variable (good/defective). In this way, the model is able to predict the label when fed with new input features. However, there are many classification algorithms with their respective hyper-parameters. In order to optimize this stage, AutoML was used to find the most suitable algorithm and its hyper-parameters [23].

Finally, the built predictive model was evaluated using flow-rate and pressure time series features from testing dataset. These quality diagnoses of the supervised ML model were compared with the FEM results, and confusion matrix and the Receiver Operating Characteristic (ROC) curve were applied to validate its performance [37].

2.1. Data acquisition

The numerical simulations of the RTM filling were carried out by the commercial software PAM-RTM®. This simulation software is based on finite element/control volume and simulates the filling stage of the RTM process basing on Darcy’s law:

$$\nu = - \frac{K}{\mu} \nabla P \tag{1}$$

where ν is the Darcy’s impregnation velocity [m/s], μ is the viscosity of the resin [Pa·s], ∇P is the pressure gradient inside the mould [Pa/m] and K is the permeability tensor of the preform [m²]. The permeability is described as the easiness of a fluid to flow through the preform.

The case study used was a thin-walled flat plate and therefore, two-dimensional analysis may be sufficient to describe the advance of the flow [38]. Since the permeability directions coincided with the global x and y directions, the permeability values k_{xx} and k_{yy} were enough to define the permeability tensor.

The used geometry was a 350 × 250 × 3 mm plate. The mesh size has a strong influence on the numerical results, so a convergence study was carried out in order to balance the resolution and computational cost. This study showed that the result converged from 10,000 elements. The geometry was meshed with 4 mm size 12,288 triangular thin shell elements. The following assumptions were made for the simulation:

- The stiffness of the mould was considered infinite.
- The preform thickness and permeability were constant.
- Race-Tracking effect (inhomogeneity in flow due to the higher permeability between the mould and the fabric) was not considered.
- The resin was incompressible.

The resin was injected from a central injection port, creating a radial flow pattern. Furthermore, four vent ports were placed in the vertexes of

Table 1 Permeability values with and without binder.

	K_{ref}	K_{bin}
Reference	HPT 610 C090	HPT 610 C090 + 15 g/m ² binder
K_{xx} [m ²]	4·10 ⁻¹¹	8·10 ⁻¹¹
K_{yy} [m ²]	5·10 ⁻¹¹	9·10 ⁻¹¹

the mould. The part was segmented into 32 zones in order to create different permeability scenarios (Fig. 2). In addition, a monitoring point was located in the middle of each zone to record pressure evolution.

The injection parameters were defined by the velocity optimization module of PAM-RTM®. This module follows the methodology described by Ruiz et al. [39] for void content reduction. By compensating the viscous and capillary forces, the void content of the part can be reduced. This balance is quantified by means of the dimensionless capillary number (Ca^*):

$$Ca^* = \frac{\mu \cdot \nu}{\gamma \cdot \cos \theta} \quad (2)$$

which depends on the resin/fibre contact angle (θ), the surface tension of the resin (γ), the viscosity of the resin (μ) and the velocity of the flow-front (ν).

The fibre used was a biaxial Non-Crimp Fabric (NCF) of 50k high resistance carbon fibre, reference HPT 610 C090 from SGL. The fibre orientation was 0/90 and surface density was 610 g/m². Permeability variation due to binder application was taken into account in the simulations. The in-plane permeability measurements for both, preform with and without binder, were carried out by means of a rectilinear and saturated injection at constant flow-rate [4]. The binder was an epoxy resin in powder state (Araldite LT 3366 BD). The applied binder amount was 15 g/m² per layer. Two different permeability values for each zone were defined [38] (Table 1); one without binder (K_{ref}) and a higher permeability with binder (K_{bin}), which is justified by the creation of new flow channels by the binder [40].

The resin used was a fast curing epoxy resin (XB 3585) and hardener (Aradur® 3475) supplied by Hunstman. The density of the mixture, 1161 kg/m³, was characterized by the standard test method for density of plastics described by ASTM D792-20 [41]. The resin was injected at 120 °C and the rheological model used as input for the simulation was provided by the manufacturer’s technical data sheet.

Contact angle between the resin and the fibre was experimentally measured by X-ray micro-computed tomography (XCT) using the technique described by Castro et al. [42]. For this purpose, a carbon wick was introduced into a glass tube, which was impregnated by the capillary effect. The sample was introduced into the XCT and allowed to obtain several images of the impregnation meniscus. After processing nine meniscus, a contact angle value between the resin and the fibre of 47.8° was obtained.

The surface tension was experimentally determined by Wilhelmy plate method [43]. This method consists on pulling a plate immersed in the resin until its emersion. Then, by measuring the difference in force before and after emersion, the surface tension value is obtained, which

Table 2
Statistical features extracted from filling time series.

Feature	Time	Frequency	Hilbert
Standard error mean	✓	✓	✓
Signal energy	✓	✓	✓
Maximum	✓	✓	✓
Minimum	✓	✓	✓
Skewness	✓	✓	✓
Kurtosis	✓	✓	✓
Standard deviation	✓	✓	✓
Variance	✓	✓	✓
Length	✓	✓	✓
Mean	✓	✓	✓
Median	✓	✓	✓
Mean second derivative	✓		
Cid ce (complexity)	✓		
Sample entropy	✓		
Augmented dickey fuller	✓		
C3	✓		
Large standard deviation	✓		
Percentile	✓		
Time_reversal_asymmetry	✓		

in this case was 57.36 N/m.

As previously mentioned, 10,014 simulations were carried out, with different permeability scenarios. The average computational time of each simulation was 6 min. The programming of these simulations was developed using Python language. The developed code allows generating inputs for each scenario, launching it and acquiring the output data in an automated way. The acquired output data were the following:

- Pressure evolution in the middle point of each zone
- Flow rate evolution
- Void content of each zone
- Filling factor of each zone

The corner zones (Z1, Z8, Z25 and Z32) were excluded in order to avoid irregularities at the vent port.

2.2. Data pre-processing

The 10,000 simulations were divided in two parts; 8000 were used for training and 2000 for testing. The time series from the simulations were pre-processed and the two-dimensional (time-dependent) time series were transformed into one-dimensional arrays (time series features). In this way, an array containing the time series features and the quality label was obtained from each simulation.

Feature extraction was performed on time series data, extracting relevant statistical features (Table 2). Time, frequency and Hilbert-frequency domains transformations were used for getting different points of view on the data. After each data transformation, numerous statistical features were extracted. For the development of the time series feature extractor, the *tsfresh* library was used as a reference, but due to disagreements in the design and implementation, a new library was developed.

After the extraction, the correlation between pairs of variables was measured, as the feature extraction process can produce highly correlated features. These features were filtered in an effort to reduce noise and obtain a simpler representation of the fabrication process.

One of the main challenges of ML models is to find the right fit and avoid underfitting and overfitting effects. The underfitting effect occurs when the model is not complex enough to identify patterns and therefore does not achieve good results when making predictions with new data. On the other hand, overfitting occurs when the model fits too closely to the known data but is not able to obtain general patterns and the predictions with new data are not as accurate. In order to optimize performance, Recursive Feature Elimination (RFE) was applied using a Random Forest classifier, identifying the most relevant features. RFE is a backward elimination technique, which consists of removing the least relevant features iteratively eliminated to find the optimal number of features [37].

2.3. Model training

Subsequently, the filtered data were used as input for the automatic model optimizer (Auto-ML), TPOT [44] and Hyperopt [45] library were used for this task. This approach simplified the data analysis process, as the phases where the most sensitive decisions taken were automated. Furthermore, as a consequence of using genetic programming, optimising multiple algorithms and doing hyper parameter combinations, the most efficient models were achieved. This optimization was performed setting an initial population of combinations of algorithms and hyper parameters, and through an iterative selection process called generations, only the most accurate pipelines were selected and evolved. When it comes to the selection process, the fitness of each pipeline was calculated on the accuracy of the 5-fold cross-validation technique of the estimator. This validation technique provides a clear indication of how well the model can generalize in a new dataset without overfitting.

The final model was analysed for the purpose of gaining insight into

the manufacturing process. The interpretation procedure was carried out focusing on the importance of each feature and the interrelations between them. Apart from the model suitability analysis, a feature importance and feature interrelation analysis were conducted.

Finally, the obtained results were minutely analysed using the domain knowledge, in order to acquire new insight into the process.

2.4. Model evaluation

Once the model was trained, it was ready for evaluation. The ML model made a good-defective prediction for each of the 2000 test simulations, based on the time series features of each simulation. Each prediction was compared with the result obtained by FEM and it was determined how the prediction had been:

- **True Positive, TP:** the ML model predicted that the part was good and matched the FEM result (no defective areas).
- **True Negative, TN:** the ML model predicted that the part was defective and matched the FEM result (at least 1 defective zone)
- **False Positive, FP:** the ML model predicted that the part was good, but was wrong, as it did not match the FEM result (at least 1 defective zone)
- **False Negative, FN:** ML model predicted that the part was defective but was wrong, as it did not match the FEM result (no defective zones).

The performance of the model was measured by the confusion matrix and the Receiver Operating Characteristic (ROC) [37]. The confusion matrix is a square matrix that compares the real label (FEM results) with the predicted label (ML results). This matrix shows the general behaviour of the model by analysing the total number of True Positive (TP), True Negative (TN), False Positive (FP) and False Negative (FN). Accuracy parameter (ACC) provides general information about how many samples were correctly classified, and it is estimated as the sum of all correct predictions (TP + TN) divided by the number of total predictions [37]:

$$ACC = \frac{TP + TN}{FP + FN + TP + TN} \quad (3)$$

ROC curve compares models based on their performance, considering True Positive Rate (TPR) and False Positive Rate (FPR), for different decision thresholds [46]. To characterize the performance of each model, the Area Under the Curve (AUC) was used. The perfect model is the one with TPR of 1 and FPR of 0, which result in a value of AUC of 1 and a random guess, shows a linear ROC curve with a value of AUC of 0.5:

$$FPR = \frac{FP}{FP + TN} \quad (4)$$

$$TPR = \frac{TP}{FN + TP} \quad (5)$$

In data analysis, all the features were not equally relevant predicting the output. Feature importance measures how relevant a feature is in building the predictive model. More a feature is used, higher the relative

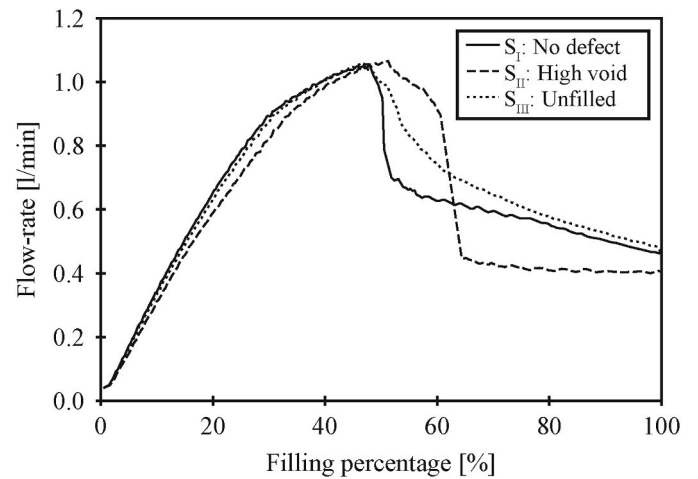


Fig. 4. Evolution of the Flow-rate with the filling.

importance. The relative importance was computed for each feature and all the features were compared between them.

3. Results and discussion

The results section is divided into four subsections according to the section defined in the methodology section.

3.1. Data acquisition

Of the 10,000 simulations performed, 5041 were labelled as good quality and 4959 as defective quality. Among the defective quality simulations, 1582 have at least 1 zone with more than 1% of void content, 1959 have dry zones and 1418 have both defects. This results on a correctly balanced dataset (almost 1:1 ratio), and it was not necessary to balance the data to prevent the model ignoring the minority class [37].

Among all the simulation, three representative results were analysed. One without any defects (S_I), another with void content higher than 1% (S_{II}) and the last with dry zone (S_{III}). The permeability map input of each simulation, which are shown in Fig. 3, generated a distinct output for each simulation.

3.1.1. Flow rate

The velocity optimizer module modified the injection parameters in order to assure the optimum capillary number, and consequently it kept the flow-front velocity at its optimum value.

Two stages can be detected by analysing the flow profile for the S_I, S_{II} and S_{III} simulations (Fig. 4). The first stage went from the beginning of the simulation to about 50% of the filling. It described the radial flow pattern of the resin before touching the nearest mould walls. If the viscosity would be constant, the flow rate increase would be linear since the perimeter of the flow-front would increase linearly. However, as the viscosity of the resin increased over time, the flow-front velocity decreased over time in order to assure the optimum capillary number. As

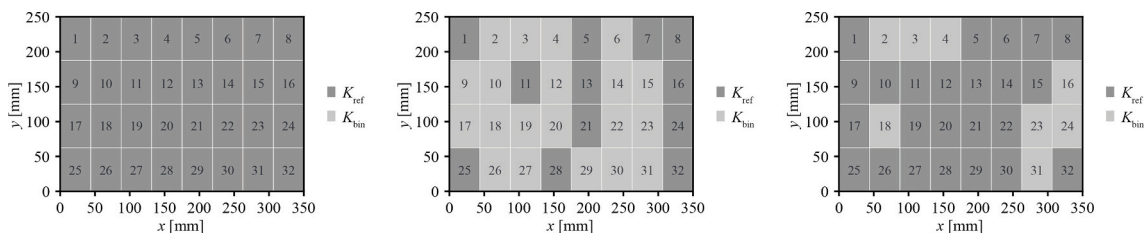


Fig. 3. Permeability map of the analysed.

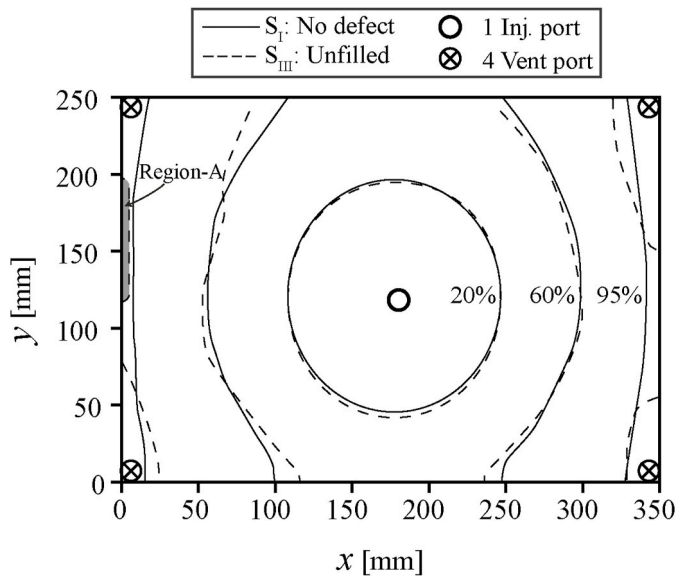


Fig. 5. The evolution of filling pattern of SI.

the optimum flow-front velocity decreased over time, the rate of change of the flow-rate also did.

In the second stage, from the moment the resin touched the wall until the complete impregnation of the mould, the flow-front area remained constant. In the same way, as the resin viscosity increased, the optimum flow-front velocity and thus the flow rate decreased.

These results confirmed that to ensure the minimum void content, a variable injection was necessary [39]. Furthermore, this variable injection was not always be the same for the identical geometry. As shown in Fig. 4, a variation in permeability affected the mould filling and therefore the injection conditions needed to be readjusted.

3.1.2. Dry zone defect

Fig. 5 shows the evolution of filling pattern of both S_I and S_{III} at 20%, 60% and 95% of the filling. At 20% of filling, both simulation followed the same pattern. Once the flow-front arrived to the closer wall, the higher local permeability in second, third and fourth zones of the S_{III} , allowed a faster flow-front as can be seen when filling is at 60%. Consequently, at 90% of filling, the fastest flow-front arrived to the vent port before total filling of the cavity and a dry zone was generated

(Region-A).

3.1.3. Void content defect

The simulations S_I and S_{II} were compared in terms of void content. As it can be seen in Fig. 6a the void content was homogeneous and generally lower than 0.5%, fulfilling the quality criteria of 1% void content in all zones. Nevertheless, in Fig. 6b a higher void content can be visualized, where a high void content band (>1.5%) stands out. The location of the band, coincide with the boundary of K_{ref} and K_{bin} zones seen in the permeability map approximately at $x = 300$ mm. It can be observed how a local variation of permeability can induce an increase in void content. In this case, the permeability variation was due to the application of binder, however, textile heterogeneities, nesting effect or race-tracking [5] could also induce local permeability variations and therefore could compromise the quality of the part in the same way.

3.1.4. Pressure evolution

Unlike recording the pressure at the injection port, the monitoring points placed in the centre of the zones can give information about the arrival time of the flow-front, its evolution and thus deduce the homogeneity of filling. It was analysed the pressure evolution in zone 13 (one of the four zones of the injection point) for the tree cases (S_I , S_{II} and S_{III}) to understand its evolution for different permeability scenarios (Fig. 7).

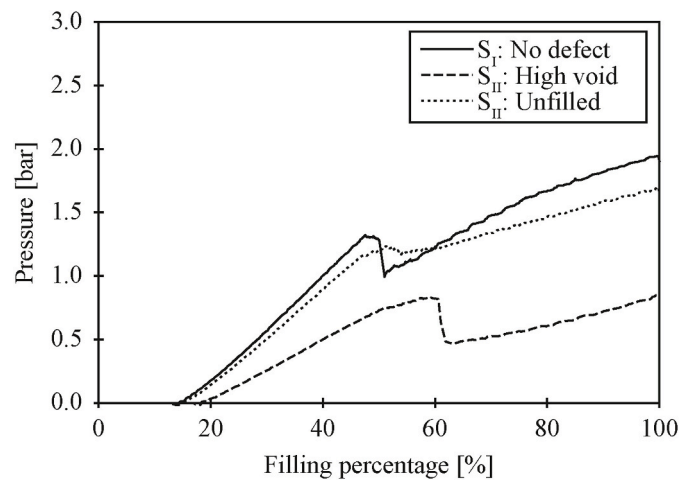


Fig. 7. The evolution of the pressure with filling in.

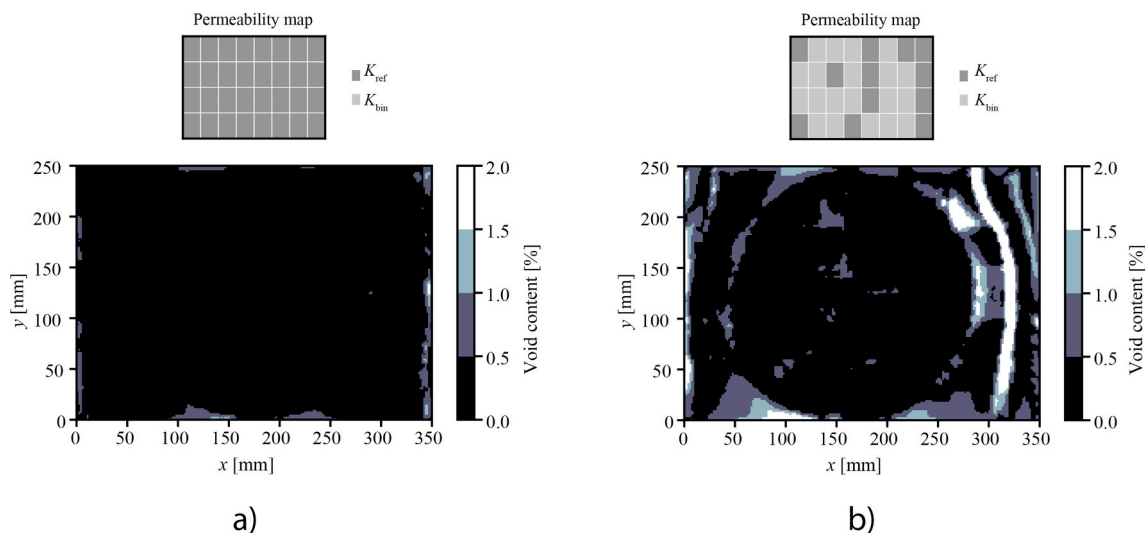


Fig. 6. Final void content of the a)SI, b)SII.

Although zones 12, 20 and 21 were as close as zone 13, zone 13 was arbitrarily chosen to analyse the overall pattern.

In all cases, once the resin reached the centre of the zone, the pressure started to increase until it reached a maximum value between 40% and 50% of the filling. This maximum coincided with the maximum injection flow rate shown in Fig. 4 and occurred when the resin reached the closest wall of the mould. The slope of pressure evolution and the instant of the peak differed in S_{II} , which was due to a higher permeability (K_{bin}) in the zones around the injection port. Then, as the area of the flow-front was reduced, the flow-rate was reduced and thus the pressure inside the cavity. The pressure started to increase again until the injection was finished, when the resin arrived to one of the four vent ports.

Each of the monitoring point recorded the arrival of the flow-front and its evolution after arrival. This information was key to identify the evolution of the flow inside the cavity and be able to determine if the part was filled correctly without defects. However, it was impossible to detect hidden patterns with the naked eye and it was necessary to apply to data analysis methods.

3.2. Data pre-processing

The large amount of data and the difficulty associated with predicting defects at a glance, automatic learning techniques were used for data analysis. Feature extraction process was applied to the time series, obtaining 8159 features for each simulation, of which lot of them were highly correlated. The features with a correlation higher than 90% were removed, leaving 1054 features for data analysis. In addition, a Recursive Feature Elimination (RFE) was applied [47], identifying that 64 was the optimum feature number.

3.3. Model training

The pre-processed data feeds the AutoML, and pipeline determined that the most accurate model was Extreme Gradient Boosting (XGB) [48]. Light Gradient Boosting Machine (LighGBM) [49], which also has a gradient boosting framework but is not included in TPOT, was included in the analysis showing also good results.

The application of the AutoML system based on TPOT genetic programming shows that ML pipelines can be improved their effectiveness in supervised classification problems, even with low prior knowledge. This can be beneficial for processes, like RTM, where no experienced data science team is available. Analysing TPOT results, it was observed that the models with the greatest predictive capacity are the so-called Ensemble Methods Based on Decision Trees. These Ensemble algorithms combines multiple models (weak learners) to obtain a more

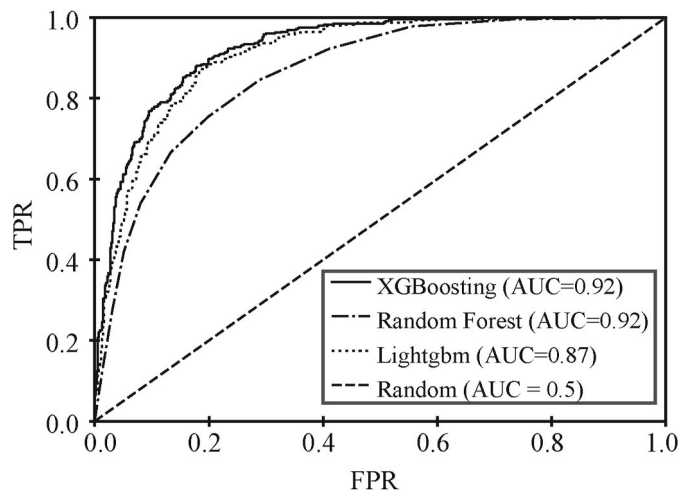


Fig. 8. Receiver operating characteristic.

robust predictive model reducing noise, bias and variance [17]. The way in which weak learners are combined varies, with Boosting and Bagging being two outstanding techniques. These methods, based on decision trees, overcome the artificial neural network (ANN) in classification problems when data come in structured rather than unstructured form (images, texts ...). This explains the fact that it is better adapted to the RTM case study where featured and structured time series are available. It is observed that both XGB and LightGBM (Gradient-Boosting method) are more robust algorithms than Random Forest (Bagging method). This agrees with the literature, since Gradient-Boosting are commonly used in predictive modelling applied to failure diagnosis [50]. Gradient-boosting methods can be better increasing accuracy and speed due to its parallel tree boosting capabilities, while bagging are better reducing overfitting.

3.4. Model evaluation

As mentioned, Extreme Gradient Boosting (XGB) [48] and Light Gradient Boosting Machine (LighGBM) [49] were selected as the most accurate models. Once the hyperparameters were optimized, both reached AUC values of 0.92 (Fig. 8).

The comparison of the optimized models showed that the XGB algorithm accuracy, 84.9% (Fig. 9a), was slightly greater than the accuracy obtained by the LighGBM model, 83.35% (Fig. 9b), both of them above 2-sigma.

Once the behavior of the model was evaluated, the cases used for this evaluation were analysed. It was observed that although the velocity optimization reduced the overall void content in all simulations, local defective zones were created. The ML model effectiveness detecting void zones was increased when the overall void content was high or there where several defective zones. When the defective zones were greater than or equal to 2, the succes rate was 98.84%, and when the overall void content was higher than 0.55% the succes rate was 100% (Fig. 10a). On the other hand, analysing the parts with unfilled zones (Fig. 10b), it can be seen that the error rate is less than 10% in both FN and FP. Moreover, over 1 unfilled zone no FP cases were found, being 100% the accuracy of the model. This showed that the model was capable of rejecting the most deviated parts and it only failed when their quality was close to the quality threshold.

All ML problems rely their prediction on data; the greater the volume of the data, the better accuracy was achieved. Fig. 11 shows the accuracy in function of training datasets volume for XGB model. As can be observed, at 4000 datasets the accuracy reached a plateau around 83%. Consequently, the 8000 datasets used for training were considered enough for the modelling.

In an attempt to understand the process, a feature importance analysis was made, by computing and gathering them by zones (Fig. 12). As can be seen, the zones 9, 16, 17 and 24, which were the last zones to be filled, had the highest importance when predicting the overall quality of the part.

In a process like RTM is not feasible to place too many sensor in the mould. Therefore, the objective should be to minimize the number of sensors without losing information about the process. For that reason, the reliability of the XGB and LighGBM models was analysed by only feeding it with the features of the aforementioned four most important zones. The number of features was reduced to 15, showing that LightGBM results were better with an accuracy of 76.7% (Fig. 13a) and an AUC of 0.87 (Fig. 13b), which is still above 2-sigma like with 32 monitoring points. LightGBM has proven to be faster in training, using less memory and getting more accuracy and coincides with the results of studies that compare gradient boosting methods [51].

In order to understand when and why the model fails, defective parts were analysed. For this purpose, the zones with excessive void and/or unfilled, as well as their position, were compared when the model was correct (TN) and when the model failed (FP) (Fig. 14). The results show that the zones furthest from the injection point are the most critical, as

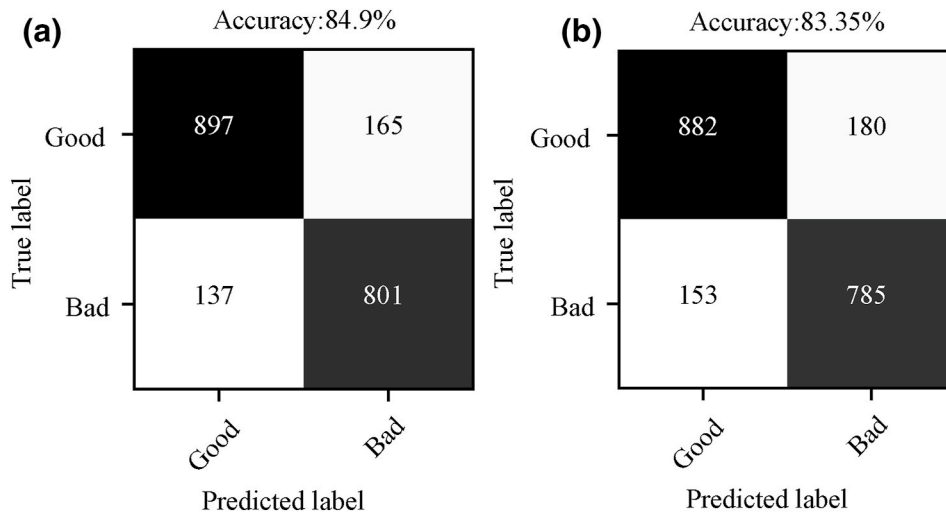


Fig. 9. Confusion matrix for a) XGB, b) LighGBM.

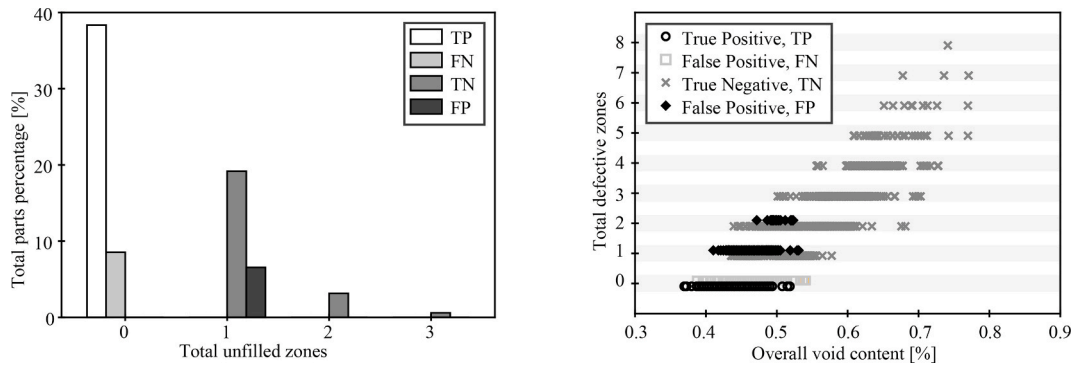


Fig. 10. a) Void quality analysis showing, b) filling quality analysis showing.

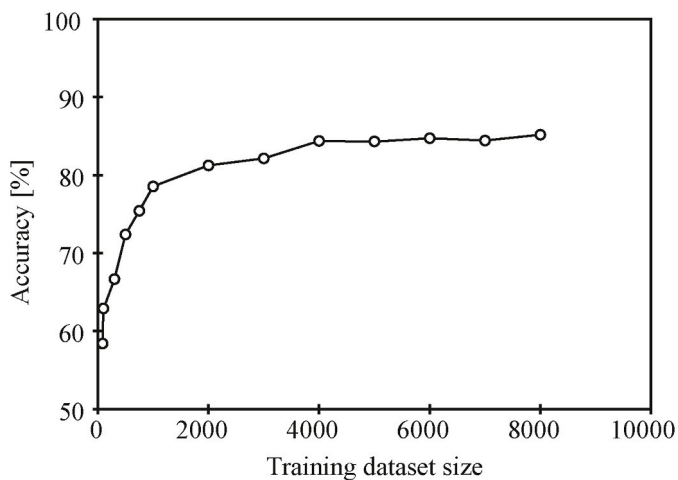


Fig. 11. Effect of the training size on.

the model does not ensure total prediction success for defects located in these zones. Nevertheless, when the NDI is needed, it may be sufficient to analyse the zones where the model can fail. Thus, ML-based NDI can be a way to reduce costs and speed up quality control process.

To obtain a more concrete result about the position of the defect, the model was scaled to the quality prediction of each zone. In this way, the model was not only able to predict the overall quality of the part but also to detect the defective zone location. As a validation, the quality of the

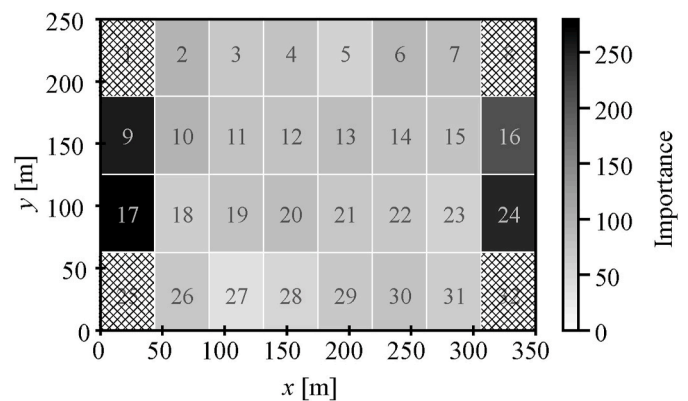


Fig. 12. Importance of each zone for quality.

S_I , S_{II} and S_{III} (analysed in the previous section) simulations was predicted.

In Fig. 15, ML and FEM results are superimposed, it can be seen how the defect predictions of the ML model matched FEM results in all cases. In the first case, S_I (Fig. 15a), the ML model correctly predicted its quality and did not predict any defective zone. In the second case, S_{II} (Fig. 15b), there were zones with high void content, and the model was able to detect such zones (Zones 7, 16, 24 and 27). Finally, in the same way, in the S_{III} simulation (Fig. 15c), the ML model is also able to detect the position of the unfilled zone (Zone 9). These results are promising as

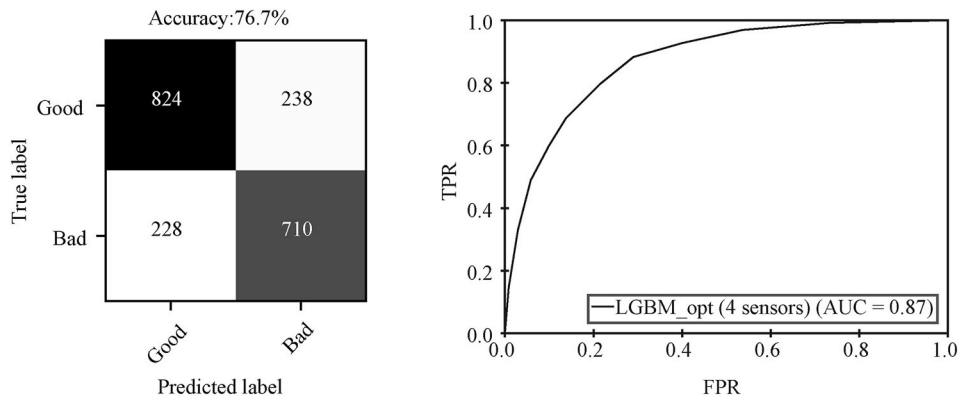


Fig. 13. LightGBM model evaluation by a).

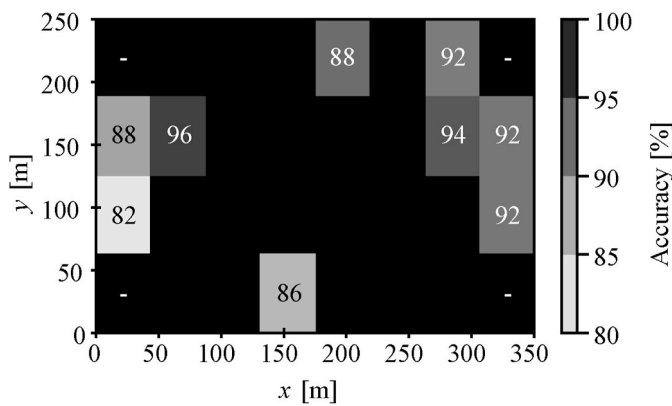


Fig. 14. Void and/or filling detecting accuracy.

they allow to detect the position of the defects in the fabricated parts. In this way, decisions such as rejecting the part or reworking the defective zones can be made and the robustness of the RTM process is improved.

Finally, the computational cost of Finite Element Method (FEM) and Machine Learning (ML) were compared. For that the average running time and data size of each simulation was compared (Table 3). It can be stated that once the ML model is trained, the predictive model reduce the computational time and storing data size comparing to FEM models. This reduction can be beneficial for its implementation in the process line where the time available for the diagnosis of each part is limited.

4. Conclusions

Part-quality after injection stage of Resin Transfer Moulding has been diagnosed based on binary classification of Supervised Learning trained with synthetic datasets. Diagnosis tools like SL are necessary,

Table 3

Computational cost of FEM method and ML method.

Method	Average running time (s)	Data size (MB)
FEM	360	27,000
ML	1	600

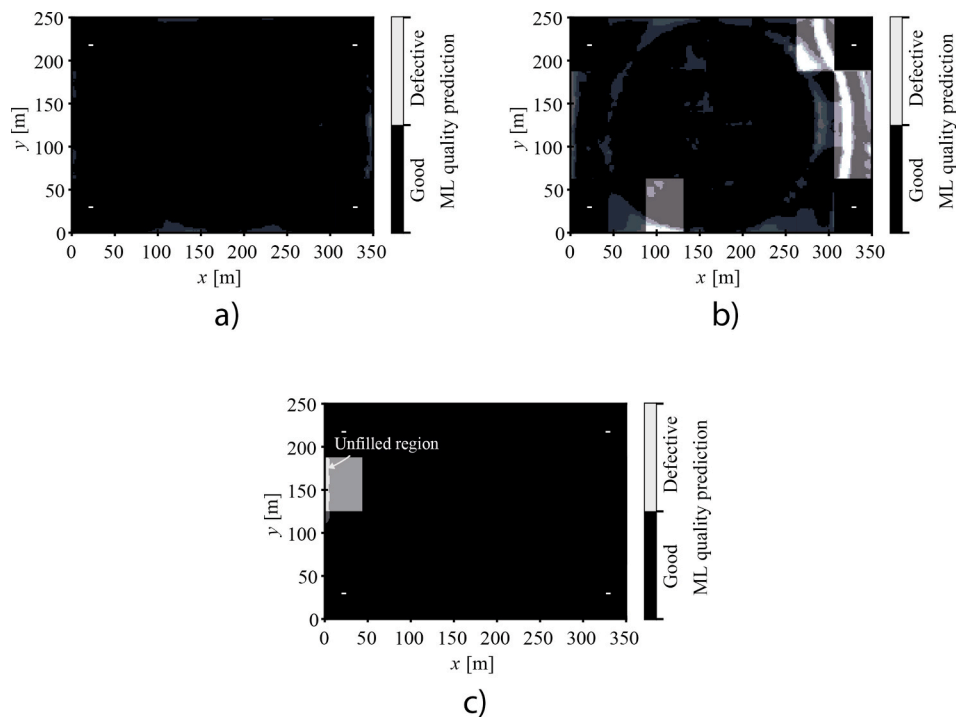


Fig. 15. Superposition of the good.

since the local permeability variability generates parts with unacceptable levels of void and/or dry zones. In fact, even if variable injection strategies for reducing void content are used, the amount of defective parts is high. Results of the 10,000 numerical simulations run with different permeability maps showed that 1582 have void content defects, 1959 have dry zone defects and 1418 have both. That is, 4959 simulations were classified as defective compared to 5041 good ones. This provided a balanced data set (with a ratio of almost 1:1) to avoid training problems in binary classification.

The algorithm and the hyper-parameters that defines the predictive model were chosen automatically by the use of TPOT and Hyperopt libraries. AutoML results showed that XGB and LightGBM were the most accurate models for predicting the filling quality of RTM, both with an AUC value of 0.92, whereas the ACC values are 84.9% and 83.35%, respectively. In this way, the application of AutoML is validated in a complex process like RTM and shows that it may useful tool for process engineers as it automates part of the pipeline. It has been demonstrated that Ensemble methods based on decision trees are the optimal ones for the selected case study, coinciding with several works of literature.

Feature importance analysis identified that the last filled zones have the highest importance when predicting the overall quality of the part. Consequently, the amount of pressure monitoring points can be reduced. The performance of the models fed with the pressure evolution of the four monitoring points located at these zones showed that LighGBM is more reliable than XGB, being its ACC 76.7% and AUC 0.87. Reducing the amount of monitoring points from 32 to 4 reduces the diagnosis quality, but it is still above 2-sigma. Another advantage of using SL instead of conventional FEM process-simulations is the lower computational cost, reducing computing time from 360 s to 1 s (after training) and reducing the data-size from 27 GB to 600 MB.

Training SL predictive models with synthetic dataset may be an effective approach to get accurate diagnosis of the impregnation quality with an accuracy above 2-sigma. The predictive model allowed the identification of the number and location of the pressure sensors in the mould, and it may be fast enough to be integrated in real process between injection and curing stages. The present case study was focus on permeability variation due to local binder content, but the methodology can be extrapolated to any other permeability variation sources, such as different fibre compaction level, nesting effect, shearing or others.

Once the injection is complete, the predictive model may be able to determine if the part is defective or not. If it is defective, the part can be rejected once it has sufficient stiffness without waiting for total curing. This might be a substantial improvement in saving time and energy to improve the robustness of the RTM process.

CRedit authorship contribution statement

J. Mendikute: Investigation, Software, Writing – original draft, Writing – review & editing. **J. Plazaola:** Investigation, Software. **M. Baskaran:** Methodology, Supervision. **E. Zugasti:** Methodology, Validation. **L. Aretxabaleta:** Supervision. **J. Aurrekoetxea:** Methodology, Supervision.

Declaration of competing interest

The authors declare that they have no known competing financial interests or personal relationships that could have appeared to influence the work reported in this paper.

Acknowledgements

J. Mendikute would like to thank the Basque Government for the predoctoral training grant (PRE_2018_1_0338). Authors would also like to acknowledge the Basque Government for providing funding support (IT833-16; KK-2017/00062) for this research.

References

- [1] González Vilatela JJ, Molina-Aldareguía JM, Lopes CS, Llorca J. Structural composites for multifunctional applications: current challenges and future trends. *Prog Mater Sci* 2017;89:194–251. <https://doi.org/10.1016/j.pmatsci.2017.04.005>.
- [2] Binetruy C. *Composites manufacturing overview of current advances and challenges for the future*. 16th Eur Conf Compos Mater ECCM 2014:22–6. 2014.
- [3] Bel S. Mechanical behaviour of non-crimp fabric (NCF) preforms in composite materials manufacturing. In: *Adv. Compos. Manuf. Process des*. Elsevier Ltd.; 2015. p. 253–68. <https://doi.org/10.1016/B978-1-78242-307-2.00012-9>.
- [4] Sozer EM, Simacek P, Advani SG. Resin transfer molding (RTM) in polymer matrix composites. In: *Manuf. Tech. Polym. Matrix compos*. Woodhead Publishing Limited; 2012. p. 245–309. <https://doi.org/10.1016/B978-0-85709-067-6.50009-2>.
- [5] Mesogitis TS, Skordos AA, Long AC. Uncertainty in the manufacturing of fibrous thermosetting composites: a review. *Compos Part A Appl Sci Manuf* 2014;57: 67–75. <https://doi.org/10.1016/j.compositesa.2013.11.004>.
- [6] Bodaghi M, Simacek P, Correia N, Advani SG. Experimental parametric study of flow-induced fiber washout during high-injection-pressure resin transfer molding. *Polym Compos* 2019;1–13. <https://doi.org/10.1002/pc.25437>.
- [7] Crane RL. Nondestructive inspection of composites. *Compr. Compos. Mater.* II 2018;7–8:159–66. <https://doi.org/10.1016/B978-0-12-803581-8.03925-4>.
- [8] Hamidi YK, Altan CM. 2.5 process-induced defects in resin transfer molded composites, vol. 2. Elsevier Ltd.; 2018. <https://doi.org/10.1016/b978-0-12-803581-8.09902-1>.
- [9] Zambal S, Eitzinger C, Clarke M, Klintworth J, Mechin P. A digital twin for composite parts manufacturing : effects of defects analysis based on manufacturing data. 2018 IEEE 16th Int. Conf. Ind. Informatics, IEEE 2018:803–8. <https://doi.org/10.1109/INDIN.2018.8472014>.
- [10] Wuest T, Irgens C, Thoben KD. An approach to monitoring quality in manufacturing using supervised machine learning on product state data. *J Intell Manuf* 2014;25:1167–80. <https://doi.org/10.1007/s10845-013-0761-y>.
- [11] Tao F, Sui F, Liu A, Qi Q, Zhang M, Song B, et al. Digital twin-driven product design framework. *Int J Prod Res* 2019;57:3935–53. <https://doi.org/10.1080/00207543.2018.1443229>.
- [12] Di Fratta C, Klunker F, Ermanni P. A methodology for flow-front estimation in LCM processes based on pressure sensors. *Compos Part A Appl Sci Manuf* 2013;47:1–11. <https://doi.org/10.1016/j.compositesa.2012.11.008>.
- [13] Di Fratta C, Koutsoukis G, Klunker F, Ermanni P. Fast method to monitor the flow front and control injection parameters in resin transfer molding using pressure sensors. *J Compos Mater* 2016;50:2941–57. <https://doi.org/10.1177/0021998315614994>.
- [14] Ding L, Shih C, Liang Z, Zhang C, Wang B. In situ measurement and monitoring of whole-field permeability profile of fiber preform for liquid composite molding processes. *Compos Part A Appl Sci Manuf* 2003;34:779–89. [https://doi.org/10.1016/S1359-835X\(03\)00121-0](https://doi.org/10.1016/S1359-835X(03)00121-0).
- [15] Gourichon B, Deléglise M, Binetruy C, Krawczak P. Dynamic void content prediction during radial injection in liquid composite molding. *Compos Part A Appl Sci Manuf* 2008;39:46–55. <https://doi.org/10.1016/j.compositesa.2007.09.008>.
- [16] Wang KS. Towards zero-defect manufacturing (ZDM)—a data mining approach. *Adv Manuf* 2013;1:62–74. <https://doi.org/10.1007/s40436-013-0010-9>.
- [17] Wuest T, Weimer D, Irgens C, Thoben KD. Machine learning in manufacturing: advantages, challenges, and applications. *Prod Manuf Res* 2016;4:23–45. <https://doi.org/10.1080/21693277.2016.1192517>.
- [18] Lu SCY. Machine learning approaches to knowledge synthesis and integration tasks for advanced engineering automation. *Comput Ind* 1990;15:105–20. [https://doi.org/10.1016/0166-3615\(90\)90088-7](https://doi.org/10.1016/0166-3615(90)90088-7).
- [19] Baturynska Ivanna, Semeniuta Oleksandr, Kw. Application of machine learning methods to improve dimensional accuracy in additive manufacturing, vol. 484; 2019. p. 114–21. <https://doi.org/10.1007/978-981-13-2375-1>.
- [20] Jain S, Shao G, Shin SJ. Manufacturing data analytics using a virtual factory representation. *Int J Prod Res* 2017;55:5450–64. <https://doi.org/10.1080/00207543.2017.1321799>.
- [21] Liu Yabansu YC, Agrawal A, Kalidindi SR, Choudhary AN. Machine learning approaches for elastic localization linkages in high-contrast composite materials. *Integr Mater Manuf Innov* 2015;4:192–208. <https://doi.org/10.1186/s40192-015-0042-z>.
- [22] Llorca J, González C, Molina-Aldareguía JM, Segurado J, Seltzer R, Sket F, et al. Multiscale modeling of composite materials: a roadmap towards virtual testing. *Adv Mater* 2011. <https://doi.org/10.1002/adma.201101683>.
- [23] Weng Z. From conventional machine learning to AutoML. *J Phys Conf Ser* 2019: 1207. <https://doi.org/10.1088/1742-6596/1207/1/012015>.
- [24] Chen CT, Gu GX. Machine learning for composite materials. *MRS Commun* 2019;9: 556–66. <https://doi.org/10.1557/mrc.2019.32>.
- [25] Wagner HNR, Köke H, Dähne S, Niemann S, Hühne C, Khakimova R. Decision tree-based machine learning to optimize the laminate stacking of composite cylinders for maximum buckling load and minimum imperfection sensitivity. *Compos Struct* 2019;220:45–63. <https://doi.org/10.1016/j.compstruct.2019.02.103>.
- [26] Gu GX, Chen CT, Buehler MJ. De novo composite design based on machine learning algorithm. *Extrem Mech Lett* 2018;18:19–28. <https://doi.org/10.1016/j.eml.2017.10.001>.
- [27] Sacco C, Baz Radwan A, Anderson A, Harik R, Gregory E. Machine learning in composites manufacturing: a case study of Automated Fiber Placement inspection. *Compos Struct* 2020;250:112514. <https://doi.org/10.1016/j.compstruct.2020.112514>.

- [28] Marani R, Palumbo D, Renò V, Galietti U, Stella E, D'Orazio T. Modeling and classification of defects in CFRP laminates by thermal non-destructive testing. *Compos B Eng* 2018;135:129–41. <https://doi.org/10.1016/j.compositesb.2017.10.010>.
- [29] Khan A, Ko DK, Lim SC, Kim HS. Structural vibration-based classification and prediction of delamination in smart composite laminates using deep learning neural network. *Compos B Eng* 2019;161:586–94. <https://doi.org/10.1016/j.compositesb.2018.12.118>.
- [30] Liu H, Liu S, Liu Z, Mrad N, Dong H. Prognostics of damage growth in composite materials using machine learning techniques. *Proc IEEE Int Conf Ind Technol* 2017; 1042–7. <https://doi.org/10.1109/ICIT.2017.7915505>.
- [31] Coelho CK, Hiche C, Chattopadhyay A. Machine learning approach to impact load estimation using fiber Bragg grating sensors. *Smart Sens Phenomena, Technol Networks, Syst* 2010;7648:764810. <https://doi.org/10.1117/12.847884>.
- [32] Brüning J, Denkena B, Dittrich MA, Hocke T. Machine learning approach for optimization of automated fiber placement processes. *Procedia CIRP* 2017;66: 74–8. <https://doi.org/10.1016/j.procir.2017.03.295>.
- [33] Wanigasekara C, Oromiehie E, Swain A, Prusty BG, Nguang SK. Machine learning based predictive model for AFP-based unidirectional composite laminates. *IEEE Trans Ind Informatics* 2020;16:2315–24. <https://doi.org/10.1109/TII.2019.2932398>.
- [34] Hürkamp A, Gellrich S, Ossowski T, Beuscher J, Thiede S, Herrmann C, et al. Combining simulation and machine learning as digital twin for the manufacturing of overmolded thermoplastic composites. *J Manuf Mater Process* 2020;4. <https://doi.org/10.3390/JMMP4030092>.
- [35] González C, Fernández-León J. A machine learning model to detect flow disturbances during manufacturing of composites by liquid moulding. *J Compos Sci* 2020;4:71. <https://doi.org/10.3390/jcs4020071>.
- [36] Wirth R. CRISP-DM : towards a standard process model for data mining. *Proc Fourth Int Conf Pract Appl Knowl Discov Data Min* 2000. 10.1.1.198.5133.
- [37] Raschka S. Python® Machine Learning 2019. <https://doi.org/10.1002/9781119557500>.
- [38] Baskaran M, Aretxabaleta L, Mateos M, Aurrekoetxea J. Simulation and experimental validation of the effect of material and processing parameters on the injection stage of compression resin transfer molding. *Polym Compos* 2018. <https://doi.org/10.1002/pc.24514>.
- [39] Ruiz E, Achim V, Soukane S, Trochu F, Bréard J. Optimization of injection flow rate to minimize micro/macro-voids formation in resin transfer molded composites. *Compos Sci Technol* 2006;66:475–86. <https://doi.org/10.1016/j.compscitech.2005.06.013>.
- [40] Dickert M, Berg DC, Ziegmann G. Influence of binder activation and fabric design on the permeability of non-crimp carbon fabrics. *Flow Process Compos Mater FPCM-* 2012;11:18.
- [41] ASTM D 792-20. Standard test methods for density and specific gravity (relative density) of plastics. *Annu Book ASTM Stand* 2020. <https://doi.org/10.1520/D0792-20>.
- [42] Castro J, Sket F, González C. S-XCT experimental determination of local contact angle and meniscus shape in liquid moulding of composites. *Compos Sci Technol* 2020;199:108362. <https://doi.org/10.1016/j.compscitech.2020.108362>.
- [43] Wilhelmy L. Ueber die Abhängigkeit der Capillaritäts-Constanten des Alkohols von Substanz und Gestalt des benetzten festen Körpers. *Ann Phys* 1863. <https://doi.org/10.1002/andp.18631950602>.
- [44] Olson RS, Moore JH. TPOT: a tree-based pipeline optimization tool for automating machine learning. 2019. https://doi.org/10.1007/978-3-030-05318-5_8.
- [45] Bergstra J, Boulevarde EHL, Yamins D, Cox DD, Boulevarde EHL. Making a science of model Search : hyperparameter optimization in hundreds of dimensions for vision architectures. *Proc. 30th Int. Conf. Mach. Learn.* 2011;28.
- [46] Bradley AP. The use of the area under the ROC curve in the evaluation of machine learning algorithms. *Pattern Recogn* 1997;30:1145–59. [https://doi.org/10.1016/S0031-3203\(96\)00142-2](https://doi.org/10.1016/S0031-3203(96)00142-2).
- [47] Pedregosa F, Varoquaux G, Gramfort A, Michel V, Thirion B, Grisel O, et al. Scikit-learn: machine learning in Python. *J Mach Learn Res* 2011.
- [48] Chen T, Guestrin C. XGBoost: a scalable tree boosting system. *Proc. ACM SIGKDD Int. Conf. Knowl. Discov. Data Min.* 2016. <https://doi.org/10.1145/2939672.2939785>.
- [49] Ke G, Meng Q, Finley T, Wang T, Chen W, Ma W, et al. LightGBM: a highly efficient gradient boosting decision tree. *Adv Neural Inf Process Syst* 2017.
- [50] Tang M, Zhao Q, Ding SX, Wu H, Li L, Long W, et al. An improved lightGBM algorithm for online fault detection of wind turbine gearboxes. *Energies* 2020;13. <https://doi.org/10.3390/en13040807>.
- [51] Zhao L, Huang Y, Xiao D, Li Y, Liu C. A novel method for induction motor fault identification based on MSST and LightGBM. 2020. p. 90–6. <https://doi.org/10.1109/sdpc.2019.00025>.